A STRUCTURED ANALYSIS OF A DAM BREAK INTO AN ENCLOSED WATER TANK: A GREEN HARBOR PERSPECTIVE FOR HARVESTING ENERGY

Cosmin KATONA[1], Carmen-Anca SAFTA[2]

In the paper, the evolution of a wave artificially produced in the laboratory by the sudden opening of a plane valve is studied numerically and experimentally. The phenomenon is equivalent to the breaking of a dam. It describes the 2D numerical model and the experimental model.

The numerical simulations are compared with the experiments in the same conditions of operation. The results are depicted as time evolution of the wave height, precise locations of velocity profiles and a set of uncertainties generated by the shock wave in terms of the enclosed environment. The results of the study show that the use of piezoelectric materials to convert the energy of small-amplitude waves into electrical energy is feasible and can be used in a possible green energy harbor.

Keywords: Dam break, numerical simulations, enclosed water tank, harvesting.

1. Introduction

The framework for ocean energy technology challenges the world to a total aim capacity of 53MW by 2050 [1]. Power capture and power conversion are considered two separate distinctive elements of a full conversion from resource to electricity by allowing a different way to evaluate the hydrodynamic efficiency of a device. Therefore, a new definition of the extracting energy from a natural resource by the interaction with a device is implemented by producing it as an input to power take-off (PTO) [2].

The propagation of waves from deep depths to shallow coastal surfaces is affected by the topography of the bottom surface resulting in wave refraction, the rolling effect and finally it's breaking. Studies of these processes are important in coastal engineering due to the significant impact of wave forces, their characteristics and sediment transport, which particularly influence coastal structures [3].

[1] Eng., PhD Std, University POLITEHNICA of Bucharest, Romania, e-mail: cosmin.katona@gmail.com
[2] Prof., PhD, University POLITEHNICA of Bucharest, Romania, e-mail: safta.carmenanca@gmail.com

In the modern world, the aspect of expanding port areas becomes a challenge due to outdated structures and the proposal of new locations become slightly sensitive when it comes to environmental protection. Thus, an opportunity to modernize coastal areas is represented by green energy. As the ports, even of small scope, cannot be moved or expanded, one method of their (ports) optimization is the capture of energy from renewable sources. The coastal area brings into view the exploitation of the micro-potential energy captured by the power of the waves.

In the present case, we have a tourist port (Tomis port, Constanța, Romania) where small and medium-sized boats are house. Once tied to the shore, reveals a relatively low electricity consumption due to sources such as the lighting system, electronic systems for emergency cases, desalinize installations and possibly air conditioning.

This port area is ideally positioned to capture wave energy as it is near the coast and thus waves generated offshore will find relatively direct trajectories to the inner harbor basin. From here, the idea of suggesting the exploitation of the existing micro-energy potential in wave transport.

A port proximity assessment together with a study of wave energy capture can generate considerable economic and financial effort. Therefore, the proposal of a numerical investigation can reduce this financial contribution and provide an overview of this complex physical phenomenon.

A simple physical starting point is the wave impact on the harbor containment structure. This impact can be evaluated as a possible energy micro potential that can support the electricity consumption required by a small size boat.

2. State of the art

A dam break flow represents a transient flow with different temporal and spatial scales associated, frequently, with dam failure risk assessment [4]. The physical phenomena expressed as a mathematical model ends up to a Riemann problem due to the uncertainties generated in the free surface flow by the instantaneous removal of a vertical barrier [5,6]. That is why numerical simulations are considered a robust tool of research in the meaning of providing complementary information for the direct, high expensive, experimental observation. By bringing the dam break physical process into an enclosed water tank, points out a new perspective with applicability to harvesting energy concept for a green harbor.

3. Governing Equations

The technical comparative highlighting is brought into the technical hydraulics plan by the case of a dam breaking. The phenomenon of breaking a dam highlights the maximum energy carried by the unsteady flow. This breaking process generates a flow wave that originates in the static domain at rest. The movement of the inverse negative wave builds up a maximum pressure point over time and upon contact with an obstacle, in this case the berth wall, it transfers energy by breaking the wave. The static flow describes a shock in the fluid once disrupted by removing a barrier producing a physical instability.

The purpose of this study is to capture this reverse negative wave breaking phenomenon through numerical methods in a small water tank facility. A theoretical starting point is the description of non-permanent free-surface motion by decomposing the negative wave into superimposed elementary waves Fig.1. Thus, we will write the continuity equation for a small, rectangular channel, which will have an elementary wave disturbance like an emptying wave [4].

The continuity equation takes the form:

$$(c+V)\cdot h = (c+V-\delta V)(h-\delta h) \tag{1}$$

Apply the momentum theorem between the same sections, as follows:

$$\rho Q(c+V-\delta V-c-V) = -\rho g(h-\delta h)^2\frac{1}{2}b + \rho g\frac{h^2}{2}b \tag{2}$$

From (1) and (2) results:

$$c = \sqrt{gh} - V \tag{3}$$

$$\delta h = -\frac{\delta V}{\sqrt{g}}\sqrt{h} \tag{4}$$

If we consider $\partial h \to 0$ and $\partial h \to dh$, the differential equation for describing the velocity in the channel has the following expression:

$$V = -2\sqrt{gh} + ct \tag{5}$$

We impose initial conditions $h = h_1$, resulting in $V = V_1$, it follows:

$$c = \sqrt{gh} - V = 3\sqrt{gh} - 2\sqrt{gh_1} - V_1 \tag{6}$$

where V_1 – represents the velocity before the disruptive moment.

Therefore, we can define the crest and trough of the wave by the following expression (Figure 1):

$$c_1 = \sqrt{gh} - V_1 \tag{7}$$

$$c_2 = 3\sqrt{gh_2} - 2\sqrt{gh_1} - V_1 \tag{8}$$

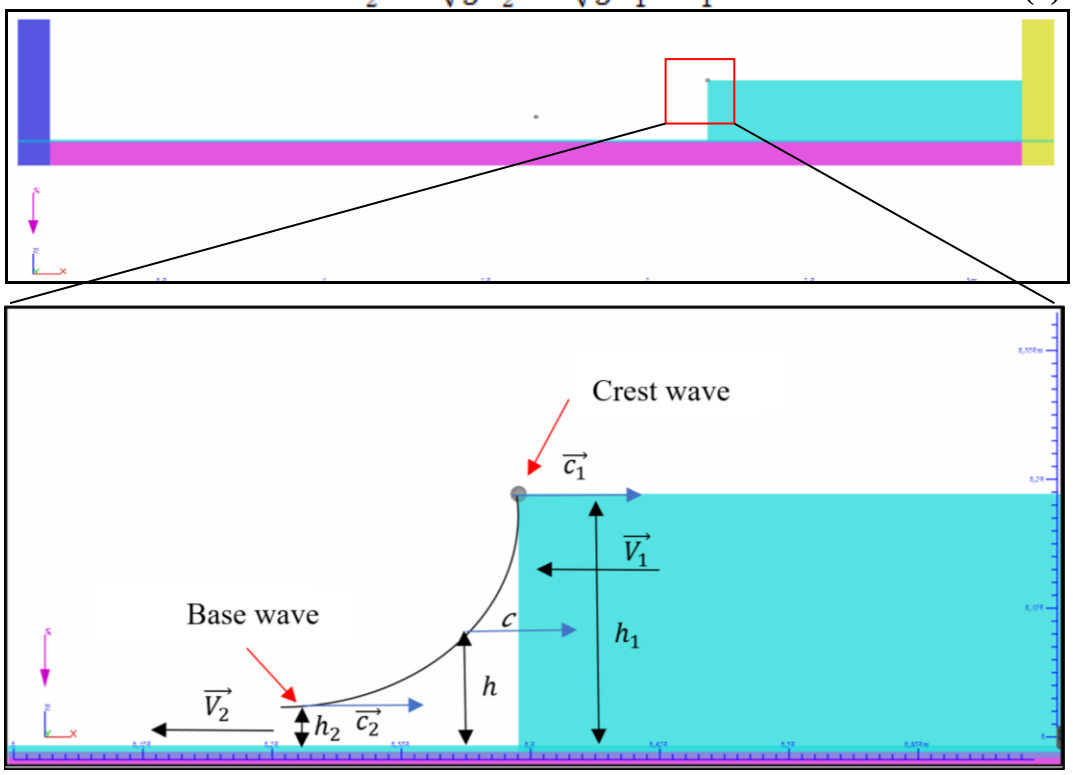

Fig. 1. The numerical domain – actual structure and boundary conditions

4. Numerical simulation

The numerical software *Flow3D* is employed for mesh generation and numerical set up. A reliable model for streamline curvature applications is chosen as *k-epsilon RNG* model. The results post processing were realized by using the *FlowSight* extension tool from the *Flow3D* software.

The domain of the numerical simulation comprises a solid domain represented by the edges of the walls and a hydrostatic fluid domain. This domain is created following the designation of the experimental stand to achieve a similarity of domains as real as possible. The disruptive part is achieved by breaking the retaining wall of the water volume like breaking a dam.

The mesh was discretized using the conformal mesh method with the application of refine regions in the sensitive areas such as the dam breaking zone of the wave, the points of maximum impact on the wall as well as the bottom area. These fine meshes can be visualized in Fig. 2.

The grid sensitivity of the mesh was made following the standard method by producing three grids, one coarse, one medium and one fine. It was observed

that the convergence result does not represent an asymptotic solution to the real solution. This sensitivity is presented in Table 1.

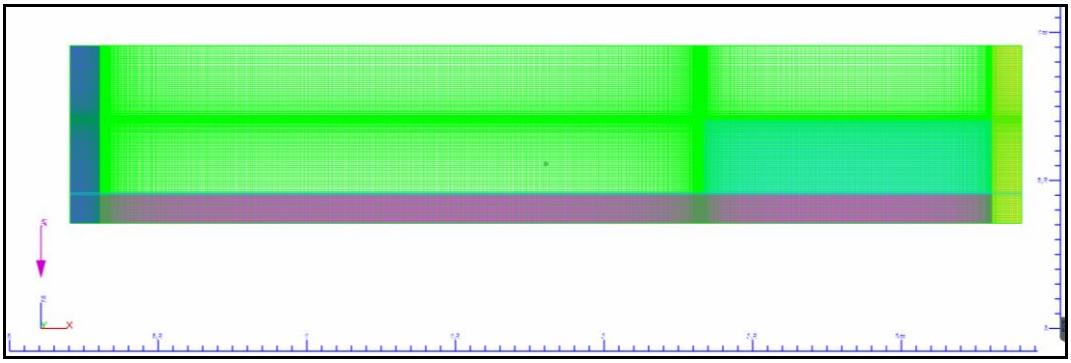

Fig. 2. The refined mesh used in the numerical simulation

The chosen turbulence model is the $k-\varepsilon\ RNG$ model because it accounts for the effect of the smallest scales of motion and allows precise accuracy for low Reynolds number cases. Compared to the standard turbulence model, it normalizes the governing Navier-Stokes equations to bring out eddy flows and accurate boundary layer exposure. Thus, $k-\varepsilon\ RNG$ turbulence model becomes a suitable candidate for boundary layer accuracy.

Table 1

Percentage error of U and k for the three different refined meshes

Refinement	Cells (Millions)	*k* % Error	U % Error	GCI k % Error	GCI U % Error
Coarse (1)	0,4	5,16	4,27	-	-
Medium (2)	1,2	3,86	2,23	(1-2) 1,82	(1-2) 3,79
Fine (3)	4,2	-	-	(2-3) 0,95	(2-3) 1,67

Additionally, the analysis of grid convergence index (GCI) between refinement meshes for turbulent kinetic energy and velocity have been computed:

$$GCI = \frac{Fs\,|e|}{r^p - 1} \tag{9}$$

where F_s is a safety factor: $F_s = 1.25$. The resulting GCI are shown in Table 1.

Following the sensitivity study grid, it was decided to use the fine resolution grid because the physical phenomenon presents elements of physical instability and to capture these sensitivities, a fine grid domain was imposed. The initial conditions were simple, namely, the fluid is in a state of hydrostatic rest so that the breaking of the negative wave can be realized immediately. Contact walls were imposed as static solids without dynamic solid-fluid interaction. The total simulated time is 15s.

The numerical scheme used in the numerical simulation of the dam break discharge wave included the following conditions:

- the calculation algorithm - implicit pressure.
- time step - Δt=0.01s.
- the customized time step in the sensitivity area of the advection gradient - Δt=0.001 s:
- viscosity tensor and free surface – explicit.
- calculation of the advection moment – second order.
- solving moment and continuity equations.

In the following paragraphs, we will present the numerical simulation results in the form of 2D graphical representations. These graphs are intended to highlight the breaking of the wave, the free surface line with the rigor heights, the fluid transport, the impact with the wall, the maximum pressure point, the stabilization, and the damping of the wave due to the closed configuration.

5. Experiment

The stand definition involved a numerical error reduction study through simple numerical simulations to detect the appearance of numerical instabilities due to the dimensions of the test stand. This numerical procedure reduces the errors of the stand dimensioning by the rounding method involving the iterative calculations of precision up to 16 significant tenths.

The numerical-experimental balance proposed in the case of wave generation by a dam break is a setup of dimensions in the form of the ratio $\frac{L}{h_{fluid}} > 6$. If the dimensioning of the basin is too small, the effect of the wave from a static position generates permanent shocks in the field which will lead to cumulatively new waves. If the dimensioning of the basin is too large, the opposite effect appears in the numerical-experimental relationship, by imposing a very large discretization domain that will lead to a much too large and inefficient calculation effort.

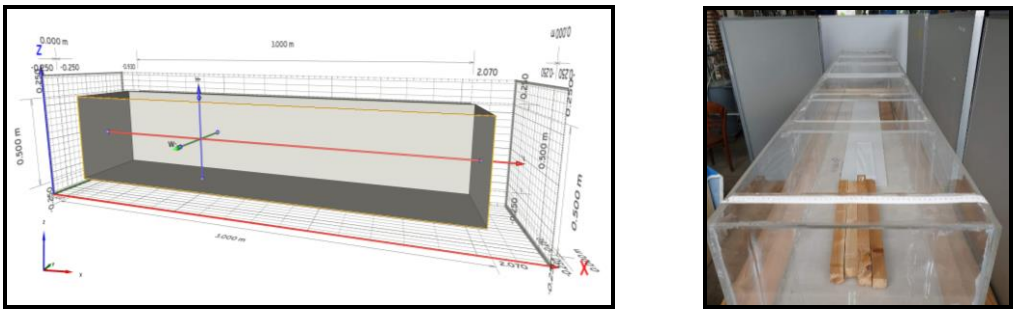

Fig. 3. Grid domain in respect with the actual stand water tank

The present case neglects the transverse axial domain of the basin, *l* because the numerical study aimed to perform numerical simulations in 2D which offers the

possibility of fine meshes with a reduced computational effort. The representation of the geometric parameters of the water tank can be seen in Figure 3.

The height of the fluid at rest (m)	The rolling of the wave from	
	Small section (1)	Big section (2)
$h_{12} = 0{,}25$	X	
$h_{21} = 0{,}30$		X
$h_{21} = 0{,}35$		X
$h_{21} = 0{,}40$		X

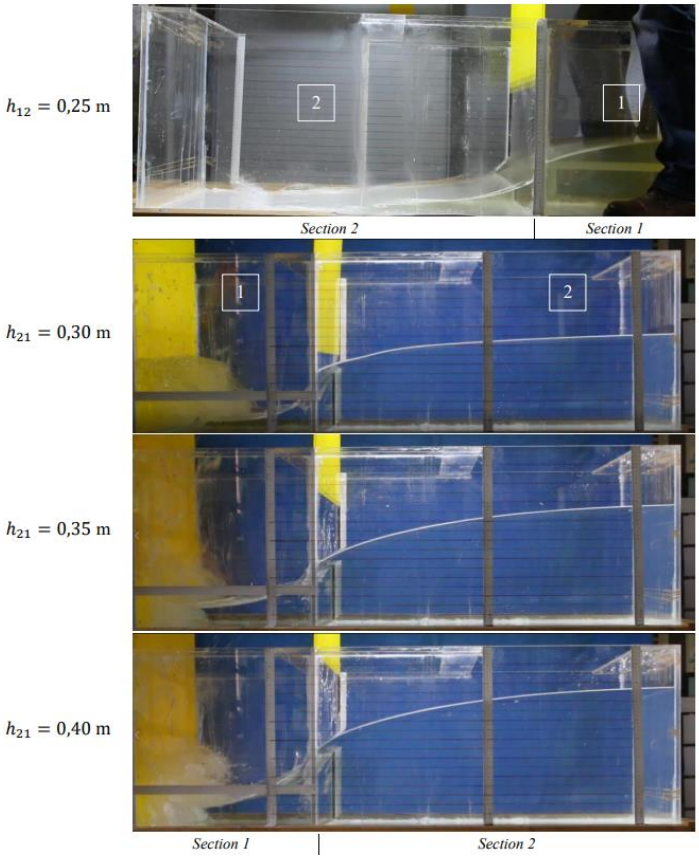

Fig. 4. The experimental cases of dam breaking wave from the small section to the large section and vice versa on the specified static heights

5. Results

The method of direct visualizations requires the comparison at different time points of the fluid flow characteristics. Digital elements were used to remove the synchronization errors between the numerical result and the experiment, and the modern recording slow-down effect was considered for these experiments.

The detailed viewpoints selected are as follows: (a) the breaking position; (b) the position of maximum impact at the wall; (c) the wall contact position.

The case chosen for the dam break validation is the case with $h_{12} = 0{,}25$m, as shown in Figure 4. This case was chosen because the volume of water is smaller and the contact effect at the wall remains within the built water tank. The height of the wave generated is measured to be 0.11 m at the first pass and then this wave decreases in intensity due to the energy dissipation through the damping effect at the wall. The dam break case by rolling from the large section into the small section presents a high-order shock compared to the previous case and the measurement of the free surface level becomes difficult, especially around maximum impact. From here, choosing the case $h_{12} = 0{,}25$m gives us the possibility of measuring the free surface through the recording device.

At the moment $t_{12} = 0.2\,s$, the wave is already breaking, and the rolling effect is taking place. This phenomenon can be visualized and distinguished from Figure 6a) and b). It is realized that the additional fine discretization mesh in the surf zone easily captures this dam break.

The maximum pressure impact and rise in the vertical axis is achieved at $t_{12} = 1{,}2\,s$. The simplicity of this impact can be seen very well in the pressure distribution on the contact wall.

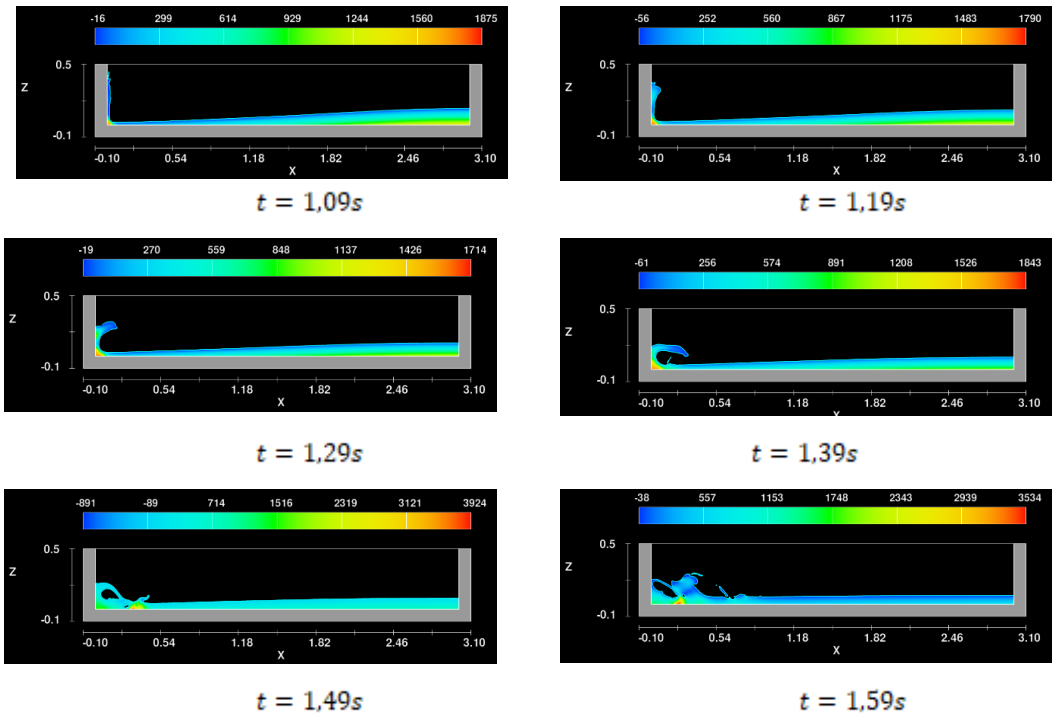

Fig. 5. The dam break wave evolution between the maximum pressure point and the reflected wave, $t = 1.09 - 1.79s$

$t_{12} = 0.2\ s$

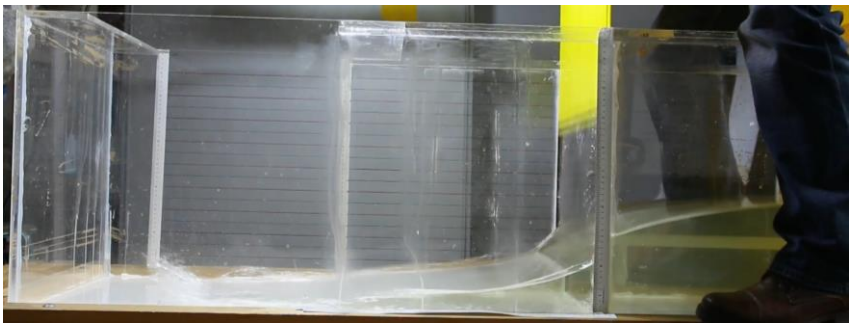

a) Experiment

b) Numerical Simulation

Fig. 6. The experimental case of breaking the emptying wave from the small section to the large section and for the static height $h_{12} = 0{,}25$ and $t_{12} = 0.2\ s$

$t_{12} = 1.2s$

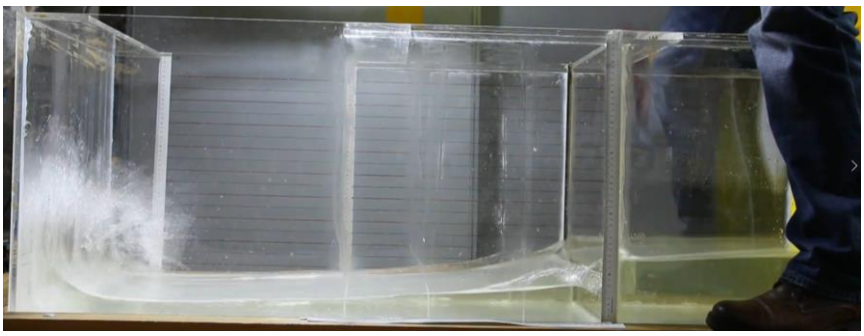

a) Experiment

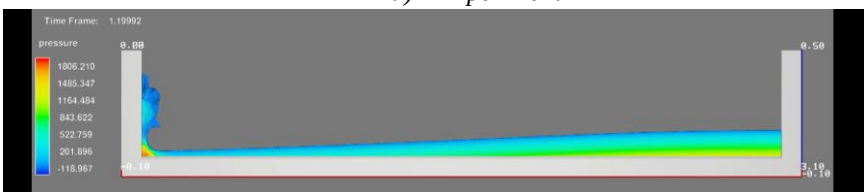

b) Numerical Simulation

Fig. 7. The experimental case of breaking the emptying wave from the small section to the large section and for the static height $h_{12} = 0{,}25$ and $t_{12} = 1{,}2\ s$

Also, the wave fading curve due to the impact with the wall begins to take considerable visual forms and the unfolding of the free surface over the entire domain is outlined.Here, we distinguish that the maximum height reached by the wave in the numerical simulation is $h_{12} = 0{,}37$m and in the experimental domain it

reaches $h_{12} = 0{,}33$m. Thus, the relative error between experiment and simulation is about 9%. This source of error cannot be eliminated due to the definition of the turbulence model used *(k-epsilon RNG*) but can be reduced. The *k-epsilon RNG* model employs a modified coefficient in the dissipation rate equation to account the interaction between the turbulent dissipation and mean shear. This coefficient is defined empirical which can generate lack of prediction for high streamline curvatures. We believe that the error can be improved by employing error function approximations. However, we believe that the numerical simulation overpredicts the point of contact with the wall. The cause error can be eliminated either by increasing the discretization grid or by using an accurate turbulence model, such as LES (Large Eddy Simulation). Reducing the time step in this turbulence model we strongly believe will not improve the results.

$t_{12} = 1{,}4\,s$

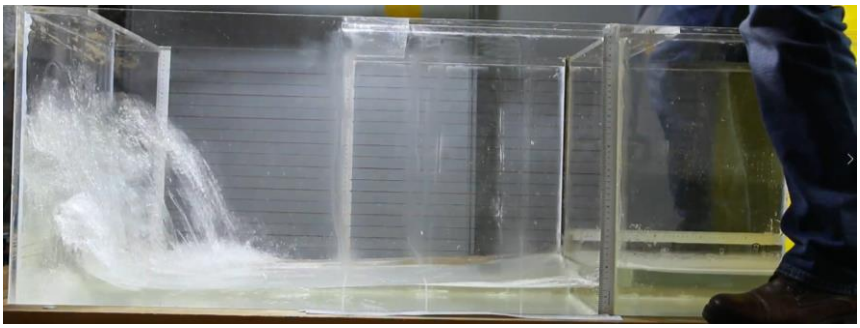

a) Experiment

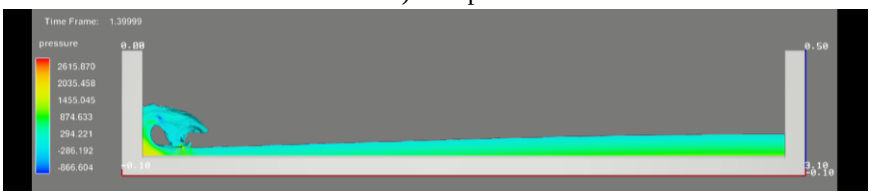

b) Numerical Simulation

Fig. 8. The experimental case of breaking the emptying wave from the small section to the large section and for the static height $h_{12} = 0{,}25$ and $t_{12} = 1.4\,s$

The impact at the opposite wall from the dam breaking point of the wave carries out an energy transfer. Thus, the wave power [14] can be expressed as follows:

$$P_{\mathbf{wave}} = 0{,}0976\gamma h^2 TL \tag{10}$$

where $\gamma -$ represents the specific gravity, $h -$wave height, $T -$wave period, $L -$ length of engaged wave front.

By extracting the values corresponding to the moment of contact with the side walls of the simulation domain, the following power micro potential was achieved:

Table 2

Potential wave power captured in respect with numerical simulations

Time scale (s)	Wave height (m)	Wave period (s)	Power wave (W)	Power conversion (W)	% capture [15]
0,9	0,49	0,9	21,04	2,32	11
4,6	0,21	3,7	16,13	1,77	11
7,8	0,1	3,2	3,1	0,34	11
11,1	0,09	3,3	2,59	0,28	11
14,5	0,07	3,4	1,6	0,17	11

Table 2 shows the captured power potential for the dam break over a 15s interval. The total captured power potential is 4.89 W. A technical configuration for achieving this capture is represented by piezoelectric materials in Figure 9.

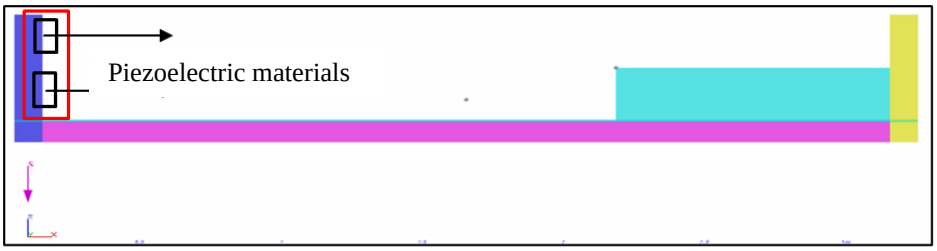

Fig. 9. A possible configuration with piezoelectric material on one side of the water tank

According to [8-13], the maximum power achieved by the best performing piezoelectric material is 120 mW as shown in Table 3. The contact surface available in the numerical simulation setup is up to 3 piezoelectric materials. But the optimal space for capturing the micro potential will be limited only to the contact of 2 piezoelectric materials. Thus, the total maximum power generated will be 840 mW.

Table 3

Potential wave power conversion by harvesting piezoelectric material

Time scale (s)	Wave height (m)	Wave period (s)	Power wave (mW)	Power conversion (mW)	Available piezoelectric materials at contact
0,9	0,49	0,9	120	240	2
4,6	0,21	3,7	120	240	2
7,8	0,1	3,2	120	120	1
11,1	0,09	3,3	120	120	1
14,5	0,07	3,4	120	120	1

6. Conclusions

The purpose of the work is to present a dam break flow phenomena with numerical simulations and experiment with similar conditions. Through numerical simulations, the waveform obtained experimentally was qualitatively verified, the quantitative verification is to be validated through an experiment and a 3D

numerical simulation and expected to increase in performance with accurate PIV measurements. The numerical simulation, the low-cost experiment and the assembly of a piezoelectric material might represent an important contribution of a future virtual laboratory.

A proposal for the placement of piezoelectric materials on the hull of the ship to achieve micro-energy potential for the purpose of the independence of the coupling to the local current distribution grid can be achieved. The integration of piezoelectric materials offers the opportunity to improve survival procedures at sea in extreme conditions of failure of operational support facilities for boats and the protection of human life at sea.

The integration of piezoelectric materials in the inner harbor area by placing them in a sector dedicated for capturing energy on the construction of the mooring berth emphasizes a reliable component of a green harbor.

R E F E R E N C E S

[1]. *** An overview of ocean energy activities in 2020 – Annual Report, Ocean Energy Systems 2020

[2]. *** An international evaluation and guidance framework for ocean energy technology, Ocean Energy Systems, 2021

[3]. *J.J. Stoker*. "Water Waves, the mathematical theory with applications". Interscience Publishers, 1957

[4]. *R. Aleixo*, "Transient flow analysis by imaging methods – Voronoi particle tracking velocimetry applied to the dam break flow", V European Conference on Computational Fluid Dynamics, ECCOMAS CFD, 2010

[5]. *R. Aleixo, S. Soares-Frazao, and Y. Zech*, Velocity-field measurements in a dam-break flow using a ptv voronoi imaging ˜ technique. Experiments in Fluids, 50:1633–1649, 2011.

[6]. *M. Gomez-Gesteira, B. D. Rogers, R. A. Dalrymple, and A. J.C. Crespo*, State-of-the-art of classical sph for free-surface flows. Journal of Hydraulic Research, 48(sup1):6–27, 2010.

[7]. *D.E. Nistoran*, et al., "Hidraulică tehnică" (Technical Hydraulics). Editura Printech București, 2007, pp.202-205.

[8]. *A. Erturk, D.J. Inman*, 10.4.4 Overall Comparision of Ceramics (PZT-5H, PZT-8) and Single Crystals (PMN-PZT, PMN-PZT-Mn). In Piezoelectric Energy Harvesting, 1st ed.; John Wiley & Sons: Hoboken, NJ, USA, 2011; pp. 315–317.

[9]. *K.A. Cook-Chennault, N. Thambi, A.M. Sastry*, Powering MEMS portable devices—A review of non-regenerative and regenerative power supply systems with special emphasis on piezoelectric energy harvesting systems. Smart Mater. Struct. 2008, 17, 043001.

[10]. *J. Feenstra, J. Granstrom, H. Sodano*, Energy harvesting through a backpack employing a mechanically amplified piezoelectric stack. Mech. Syst. Signal Process. 2008, 22, 721–734.

[11]. *J. Liu, W.J. O'Connor, E. Ahearne, G. Byrne*, Electromechanical modelling for piezoelectric flextensional actuators. Smart Mater. Struct. 2013, 23, 025005.

[12]. *Y. Wang, W. Chen, P. Guzman*, Piezoelectric stack energy harvesting with a force amplification frame: Modeling and experiment. J. Intell. Mater. Syst. Struct., 27, 2324–2332, 2016.

[13]. *H. Li, C. Tian, Z.D. Deng*, Energy harvesting from low frequency applications using piezoelectric materials. Appl. Phys. Rev. 2014, 1, 041301.

[14]. *C. Iulian*, "Utilizarea energiei valurilor", (Use of Wave Energy), Ed. Tehnica, 1990.